Int. J. Electrochem. Sci., 12 **(2017)** 7404 – 7410, doi: 10.20964/2017.08.62

International Journal of
ELECTROCHEMICAL
SCIENCE
www.electrochemsci.org

Short Communication

Pulsed Laser Deposited SnS-SnSe Nanocomposite as a New Anode Material for Lithium Ion Batteries

Kaiyuan Wei[1,2], *Yu Zhao*[1], *Jiabin Liu*[1], *Shengzhou Liu*[3], *Yixiu Cui*[1], *Rongtao Zhu*[2], *Yin Yang*[3,*], *Yanhua Cui*[1,*]

[1] Institute of Electronic Engineering, China Academy of Engineering Physics, Mianyang 621000, P. R. China
[2] School of Chemical Engineering & Technology, China University of Mining and Technology, Xuzhou 221116, P. R. China
[3] Institute of Advanced Synthesis, School of Chemistry and Molecular Engineering, Jiangsu National Synergetic Innovation Center for Advanced Materials, Nanjing Tech University, Nanjing 211816, P. R. China
[*]E-mail: ias_yyang@njtech.edu.cn (Y. Yang); cuiyanhua@netease.com (Y. Cui)

Received: 10 May 2017 / *Accepted:* 14 June 2017 / *Published:* 12 July 2017

SnS-SnSe nanocomposite thin films are successfully fabricated by pulsed laser deposition (PLD) method and their electrochemical properties are investigated by cyclic voltammetry (CV) and discharge/charge measurements. SnS-SnSe composite electrode delivers an initial discharge capacity of 1225 mAh/g, which is 1.8 and 2.6 times of SnS and SnSe thin film electrodes, respectively. The high capacity of composite electrode is speculated to be related to its large amounts of grain boundaries which can store more Li. Mechanistic study based on CV and *ex situ* X-ray diffraction (XRD) results imply that SnS-SnSe composite decomposes to generate nanaosized Li_xSn, Li_2S and Li_2Se during initial discharge process, which then form Sn_2SSe single phase instead of composite phase upon charge process. The subsequent cycles are based on reversible electrochemical reaction between Sn_2SSe phase and metallic Li.

Keywords: SnS-SnSe nanocomposite; Anode; Lithium ion batteries

1. INTRODUCTION

Tin-based compounds have been receiving extensive research interests as alternatives of graphite to be used as anode materials for lithium ion batteries (LIBs), due to the fact that Sn can alloy with Li and provide extremely large specific capacity of 994 mAh/g (based on $Li_{4.4}Sn$ electrochemistry) [1-6]. Unfortunately, the significant volume expansion of 358% during alloy-dealloy

process leads to fast capacity decay of Sn-based compounds and therefore hinders their practical use [7-8]. Thanks to the efforts from many research groups, various strategies have been developed to address the volume expansion issue, including reducing particle size of active material [9-11], introducing an inactive matrix to buffer the stress between particles [12-14], employing composite instead of pure material as electrode [15-17], and so on.

As two important II-VI semiconductors, SnS and SnSe with orthorhombic crystal structure have attracted considerable research interests as anode for LIBs because of their unique physical and chemical properties [18-21]. Although these two anode materials deliver large capacities during the initial a few cycles, the values rapidly fall into the range of less than 400 mAh/g. In order to improve cycling performance of tin-based compunds and develop long-life anode material with large capacity, herein we prepare SnS-SnSe nanocomposite films by pulsed laser deposition (PLD) method and investigate their electrochemical properties. The results show that the SnS-SnSe nanocomposite electrode exhibits relatively large capacity and stable cycling capability, making it a promising anode candidate for LIBs.

2. EXPERIMENTAL

SnS-SnSe thin films were fabricated by pulsed laser deposition (PLD) method. The target was made by mixing high-purity of Sn, S and Se powder (all 99.9%) with molar ratio of 2:1.2:1.2. The mixture was then grounded by pestle and mortar and pressed to form a pellet with diameter of 13 mm as the target. The following deposition condition is used to prepare SnS-SnSe thin films. A 355 nm laser beam provided by the third harmonic frequency of a Q-Switched Nd:yttrium aluminum garnet (YAG) laser (Quanta-Ray GCR-150) with a repetition rate of 10 Hz and a pulsed width of 5 ns was focused on the rotating target. The angle between the laser beam and surface of the target was set at 45º and energy density of the laser was set at 2 $J \cdot cm^{-2}$. The distance between the target and stainless steel substrate was set to 38 mm. The vacuum was kept at a pressure of 2×10^{-3} Pa and the substrate temperature was kept at 200 ºC during deposition for 0.5 h. After the deposition, the film was held at 200 ºC for an extra hour annealing. As a comparison, SnS and SnSe thin films were also prepared by using the same method with Sn/S mixture (molar ratio 1:1.2) and Sn/Se mixture (molar ratio 1:1.2) target, respectively.

Weight of the thin films were gained by measuring the difference of substrate before and after film deposition via electrobalance (BP 211D, Sartorius). X-ray diffraction (XRD) patterns of thin film electrode were measured by a Bruker D8 advance diffractometer equipped with Cu Kα radiation (λ=1.5406 Å).

A three-electrode system was used for the electrochemical testing experiments. The as-deposited thin film was employed as working electrode and two sheets of high-purity lithium were employed as reference and counter electrodes, respectively. 1 M $LiPF_6$ dissolved in ethylene carbonate (EC) and dimethyl carbonate (DMC) with volume ratio of 1:1 was used as electrolyte (Merck). The cells were assembled in an argon-filled glove box. Charge-discharge measurements were conducted at

room temperature with a Land BT 1-40 battery test system. Cyclic Volatmmogram (CV) tests were taken with a scanning rate of 0.1 $mV \cdot s^{-1}$ on a CHI660A electrochemical working station.

3. RESULTS AND DISCUSSION

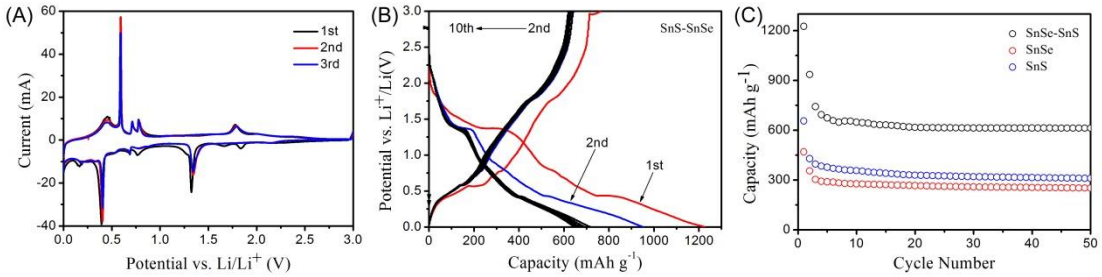

Figure 1. (A) The initial three CVs of SnS-SnSe electrode at a scan rate of 0.1 mV/s; (B) Galvanostatic charge-discharge profiles of SnS-SnSe electrode at 3μA/cm^2; (C) Cycling performance of SnS-SnSe composite and SnS, SnSe pure phase electrodes.

Figure 1(A) shows the initial three cyclic voltammograms of SnS-SnSe nanocomposite electrode in the voltage range of 0-3.0 V. It is observed that for the initial scan, a reduction peak with a shoulder appears at ~1.32 V, indicating the conversion of SnS-SnSe composite to Sn, Li_2S and Li_2Se. Upon further discharge, the reduction peaks at 0.77, 0.67, 0.40 and 0.16 V could be attributed to the alloy reaction of Sn with Li to form Li_xSn ($x \geq 4.4$) [19]. Accordingly, the oxidation peaks at 0.45, 0.59, 0.71 and 0.78 V should result from dealloying reaction of Li_xSn. A single oxidation peak without shoulder appears at 1.78 V, suggesting the formation of a single Sn_2SSe phase instead of SnS-SnSe nanocomposite. This point is further supported by the disappearance of the shoulder for the reduction peak at 1.32 V during the 2nd and subsequent scans. Note that the oxidation/reduction peaks are almost identical for the 2nd and 3rd cycles, indicating good reversibility of SnS-SnSe nanocomposite electrode.

The galvanostatic cycling profiles of SnS-SnSe/Li cell cycled between 0.01 V and 3.0 V under current density of 3μA/cm^2 are shown in Figure 1(B). The discharge/charge curves can all divided into two regions. The voltage region above 1.0 V corresponds to conversion reaction between SnS-SnSe nanocomposite (or Sn_2SSe) and Li while the region below 1.0 V results from alloy reaction between Sn and Li, which is in good agreement with CV results. The initial discharge and charge capacities are 1225 and 765 mAh/g. The large irreversible capacity could be attributed to the formation of SEI on the electrode surface during the first cycle. Figure 1(C) presents cycling performance of SnS-SnSe nanocomposite electrode. Cycling data for single phases of SnS and SnSe thin film are also plotted for comparison. As can be observed, SnS-SnSe nanocomposite experiences severe capacity loss during the first two cycles and then displays relatively stable discharge capacity. After 50 cycles, a reversible capacity of 613 mAh/g is retained, which is still significantly larger than that of commercialized graphite anode (372 mAh/g). Many researchers have synthesized SnS and SnSe materials with different sizes (from nano to micro scale) and shapes (nanoflowers, nanosheets, nanorods, etc.). The lithium storage properties of these SnS, SnSe and their composite materials have

been investigated. Table 1 lists the typical SnS, SnSe and related composites reported previously and compares their electrochemical properties with SnS-SnSe nanocomposite electrode in this work. It is clearly observed from the table that under current density of 3 $\mu A/cm^2$ (corresponds to 150 mA/g based on the mass of composite thin film), SnS-SnSe nanocomposite thin film electrode here exhibits comparable performance with the state-of-art Sn-based comapounds, which shows better cycling stability than most of previously reported SnS, SnSe and their composites, demonstrating the superior design strategy of SnS-SnSe composite electrode. Moreover, the SnS-SnSe composite electrode delivers much higher initial capacity than SnS and SnSe thin film electrode prepared by PLD (655 mAh/g for SnS and 469 mAh/g for SnSe). It is speculated that the much higher capacity of composite electrode than those of single phase electrodes lies in the fact that composite electrode possesses more grain boundaries than single phase electrode. These grain boundaries can not only facilitate Li^+ diffusion in the electrode, but also provides large quantity of interfaces for Li storage [22-24]. These synergetic effects contribute to the great enchantment in capacity for SnS-SnSe nanocomposite electrode. The capacities of SnS and SnSe electrode after 50 cycles only preserve 310 and 251 mAh/g, respectively, further confirming the argument that SnS-SnSe nanocomposite improve electrochemical performance of single phases of SnS and SnSe.

Table 1. Comparison of electrochemical performance of SnS-SnSe nanocomposite with other reported materials

Typical Materials	Current density	Initial capacity	Cycle number	Remaning capacity	Reference
SnS nanoflowers	50 mA/g	1050 mAh/g	30	500 mAh/g	[25]
3D-hierarchical SnS nanostructure	100 mA/g	1153 mAh/g	50	410 mAh/g	[26]
SnS nanosheet bonded with graphene	100 mA/g	1625 mAh/g	100	560 mAh/g	[27]
SnS nanorods/graphene composite	160 mA/g	1897 mAh/g	50	602 mAh/g	[28]
SnS/graphene nanocomposite	50 mA/g	1459 mAh/g	50	535 mAh/g	[29]
SnSe thin-film	130 mA/g	681 mAh/g	40	400 mAh/g	[30]
SnSe/carbon nanocomposite	500 mA/g	1097 mAh/g	100	633 mAh/g	[31]
SnSe-amorphous carbon nanocomposite	100 mA/g	885 mAh/g	200	626 mAh/g	[32]
SnSe nanocrystal-carbon fabric electrode	200 mA/g	1216 mAh/g	80	676 mAh/g	[21]
SnSe nanosheets	50 mA/g	1009 mAh/g	20	73 mAh/g	[33]
Se-doped SnS@carbon nanofibers	200 mA/g	1328 mAh/g	50	742 mAh/g	[34]
SnS-SnSe nanocomposite	3 $\mu A/cm^2$ (150 mA/g)	1225 mAh/g	50	613 mAh/g	This work

In order to investigate the electrochemical reaction mechanism of SnS-SnSe nanocomposite with lithium, *ex situ* XRD measurement was performed. Figure 2 presents XRD patterns of pristine

SnS-SnSe composite film and also the lithiated (discharged to 0.01 V) and delithiated (recharged to 3.0 V) films. Two diffraction peaks located at 43.4º and 50.4º come from the stainless steel substrate (marked with asterisks). For the pristine film, XRD pattern shows two major peaks at 30.6º and 31.9º, which can be assigned to (040) reflection of SnSe (JCPDS 35-1042) and (040) reflection of SnS (JCPDS 32-1361), respectively. A small amount of Sn impurity is also detected in the pristine composite film. After discharging the cell to 0.01 V, diffraction peaks of SnS and SnSe vanishes, demonstrating the decomposition of SnS-SnSe composite. Three new peaks centered at 32.9 º, 35.3 º and 47.7 º appear, which can be indexed to tetragonal Sn (JCPDS 18-1380). The presence of residual Sn in discharge products is a common phenomenon for SnS and SnSe electrodes, as reported in previous literatures [30,35]. No diffraction peaks related to Li_2S, Li_2Se or Li-Sn alloys are detected probably due to their sizes are less than X-ray coherence length (6 nm),which could not be identified by XRD technique. After recharging the cell back to 3.0 V, the peaks of tetragonal Sn disappears, suggesting the reconstruction of Sn with Li_2S and Li_2Se. No diffraction peaks corresponding to the newly formed phase is observed, an indication of its tiny small crystallized size or even amorphous phase.

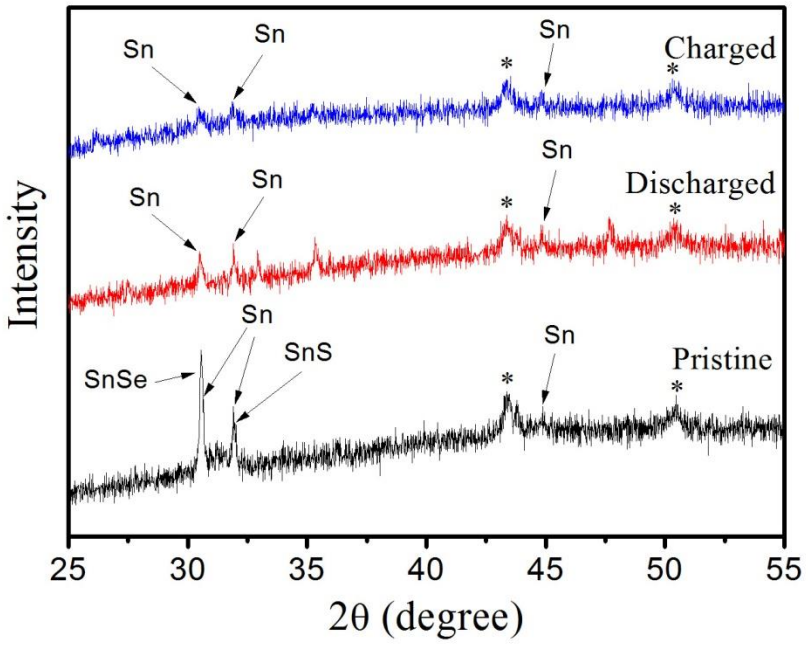

Figure 2. XRD patterns of SnS-SnSe composite electrode at pristine, discharged and charged states during the initial cycle (The peaks from stainless steel substrate are marked with asterisks).

Based on the aforementioned data, the electrochemical reaction mechanism of SnS-SnSe nanocomposite with Li involving following steps is proposed.

Initial discharge process:

$$SnS\text{-}SnSe\ (crystalline) + 4Li \rightarrow 2Sn + Li_2S\ (nanosized) + Li_2Se\ (nanosized) \quad (1)$$

$$Sn + xLi \rightarrow Li_xSn\ (nanosized) \quad (2)$$

Subsequent cycles:

Li_xSn (nanosized) ↔ Sn + xLi (3)

$2Sn + Li_2S$ (nanosized)+ Li_2Se (nanosized) ↔ Sn_2SSe (nanosized) + 4Li (4)

During the initial discharge process, crystalline SnS-SnSe composite reacts with Li to generate tetragonal Sn, nanosized Li_2S and Li_2Se phases through equation (1), followed by the alloy reaction of Sn with Li to form nanosized Li_xSn (equation 2). As a result, no diffraction peaks except for tetragonal Sn and residual Sn from pristine film are detected for XRD pattern of discharged electrode. Meanwhile, reduction peak corresponding to decomposition of SnS and SnSe in the composite can be distinguished for the initial CV curve. At the beginning stage of charge process, Li_xSn is dealloyed to produce Sn (equation 3), which then react with Li_2S and Li_2Se to generate a single phase of nanosized Sn_2SSe instead of the original SnS-SnSe composite phase (equation 4). This argument is supported by the absence of Sn_2SSe diffraction peak in XRD data for charged state and the appearance of a singlet oxidation peak above 1.0 V in CV curves. For the subsequent cycles, the reversible electrochemistry is involving reactions between Sn_2SSe with Li through equations (3) and (4). Compared with elemental Sn electrode, SnS-SnSe nanocomposite provides intermediate phases of nanosized Li_2S and Li_2Se during electrochemical reactions, which can buffer or restrain the huge structural change resulted from volume expansion due to alloy reaction of Sn with Li. If compared with single phase electrode of SnS or SnSe, SnS-SnSe nanocomposite possesses large quantities of grain boundaries, which provide more diffusion pathway for Li^+ ions and reserve extra Li within the material. Collectively, SnS-SnSe nanocomposite not only displays higher capacity than SnS or SnSe but also exhibits better cycling stability than Sn, making it a promising candidate for high energy anode materials.

4. CONCLUSION

SnS-SnSe nanocomposite has been successfully prepared by PLD method and employed as anode material for LIBs. The composite electrode shows superior electrochemical performance to single phase of SnS or SnSe, with an extremely large initial discharge capacity of 1225 mAh/g and relatively high reversible capacity of over 600 mAh/g after 50 cycles. The improvement of SnS-SnSe nanocomposite in capacity is ascribed to the existence of large amount of grain boundaries, which can facilitate Li^+ diffusion and Li accommodation. The reaction mechanism of SnS-SnSe nanocomposite with Li has been studied by CV and *ex situ* XRD measurement. It is found that SnS-SnSe composite decomposes to form nanosized Li_2S, Li_2Se and Li_xSn alloy during initial discharge process, which then involve generating nanosized Sn_2SSe single phase upon charge process. The subsequent cycles are based on the electrochemistry between Sn_2SSe and Li. This study suggests that SnS-SnSe nanocomposite is a quite promising candidate for anode material of LIBs in future.

ACKNOWLEDGEMENTS

We grateful acknowledge the financial support of LPMT, CAEP (ZZ16002). We also thank the Start-up Grant (39837127) from Nanjing Tech University and financial support from SICAM Fellowship by Jiangsu National Synergetic Innovation Center for Advanced Materials and General Financial Grant from the China Postdoctoral Science Foundation (2015M581901).

References

1. L.H. Liu, F. Xie, J. Lyu, T.K. Zhao, T.H. Li, B.G. Choi, *J. Power Sources*, 321 (2016) 11.
2. Y. Zhao, X.F. Li, B. Yan, D.J. Li , S. Lawes, X.L. Sun, *J. Power Sources*, 274 (2015) 869.
3. J.S. Chen, X.W. (David) Lou, *Small*, 9 (2013) 1877.
4. Y.F. Deng , C.C. Fang, G.H. Chen, *J. Power Sources*, 304 (2016) 81.
5. J. Hassouna, B. Scrosati, *J. Electrochem. Soc.*, 162 (2015) A2582.
6. M. Zhang, T. Wang, G. Cao, *Int. Mater. Rev.*, 60 (2015) 330.
7. J.O. Besenhard, J. Yang, M. Winter, *J. Power Sources*, 68 (1997) 87.
8. J.T. Vaughey, J. O'Hara, M.M. Thackeray, *Electrochem. Solid-State Lett.*, 3 (2000) 13.
9. H. Li, Q. Wang, L. Shi, L. Chen, X. Huang, *Chem. Mater.*, 14 (2002) 103.
10. M.S. Park, G.X. Wang, Y.M. Kang, D. Wexler, S.X. Dou, H.K. Liu, *Angew. Chem. Int. Ed.*, 46 (2007) 764.
11. X. Liu, J. Zhang, W. Si, L. Xi, S. Oswald, C. Yan, O.G. Schmidt, *Nanoscale*, 7 (2015) 282. `
12. J.M. Tarascon, M. Armand, *Nature*, 414 (2001) 359.
13. J. Zhang, L.B. Chen, C.C. Li, T.H. Wang, *Appl. Phys. Lett.*, 93 (2008) 264102.
14. Y. Yu, C.H. Chen, Y. Shi, *Adv. Mater.*, 19 (2007) 3541.
15. T. Chen, S. Wang, Z. Yang, Q. Feng, X. Sun, L. Li, Z.S. Wang, H. Peng, *Angew. Chem. Int. Ed.*, 50 (2011) 1815.
16. W. Zhou, C. Cheng, J.P. Liu, Y.Y. Tay, J. Jiang, X.T. Jia, J.X. Zhang, H. Gong, H. H. Hng, T. Yu and H.J. Fan, *Adv. Func. Mater.*, 21 (2011) 2439.
17. X.Y. Xue, Z.H. Chen, L.L. Xing, S. Yuan, Y.J. Chen, *Chem. Commun.*, 47 (2011) 5205.
18. J.J. Cai, Z.S. Li, P.K. Shen, *ACS Appl. Mater. Interfaces*, 4 (2012) 4093.
19. A.M. Tripathi, S. Mitra, *RSC Adv.*, 4 (2014) 10358.
20. L. Zhang, L. Lu, D.C. Zhang, W.T. Hu, N. Wang, B. Xu, Y.M. Li, H. Zeng, *Electrochim. Acta*, 209 (2016) 423.
21. X.F. Wang, B. Liu, Q.Y. Xiang, Q.F. Wang, X.J Hou, D. Chen, G.Z. Shen, *ChemSusChem.*, 7 (2014) 308.
22. R. Liu , S.Q. Zhao , M.M. Zhang , F. Feng, Q. Shen, *Chem. Commun.*, 51 (2015) 5728.
23. W.P. Kang, Y.B. Tang, W.Y. Li, X. Yang, H.T. Xue, Q.D. Yang, C.S. Lee, *Nanoscale*, 7 (2015) 225.
24. E.Z. Liu, J.M. Wang, C.S. Shi, N.Q. Zhao, C.N. He, J.J. Li, J.Z. Jiang. *ACS Appl. Mater. Interfaces*, 6 (2014) 18147.
25. D.D. Vaughn, O.D. Hentz, S.R. Chen, D.H. Wang, R.E. Schaak, *Chem. Commun.*, 48 (2012) 5608.
26. S.K. Li, J.X. Zheng, Z.X. Hu, S.Y. Zuo, Z.G. Wu, P.X. Yan, F. Pan, *Rsc Adv.*, 5 (2015) 72857.
27. S.K. Li, J.X. Zheng, S.Y. Zuo, Z.G. Wu, P.X. Yan, F. Pan, *Rsc Adv.*, 5 (2015) 46941.
28. A.M. Tripathi, S. Mitra, *Rsc Ad.v*, 5 (2015) 23671.
29. H.C. Tao, X.L. Yang, L.L. Zhang, S.B. Ni, *J Electroanal. Chem.*, 728 (2014) 134.
30. M.Z. Xue, J. Yao, S.C. Cheng, Z.W. Fu, *J. Electrochem. Soc.*, 153 (2006) A270.
31. Z.A. Zhang, X.X. Zhao, J. Li, *Electrochim. Acta*, 176 (2015) 1296.
32. D.H. Lee, C.M. Park, *ACS Appl. Mater. Interfaces*, 9 (2017) 15439.
33. S.Z. Kang, L.D. Jia, X.Q. Li, Y.X. Yin, L. Li, Y.G. Guo, J. Mu, *Colloid. Surface A*, 406 (2012) 1.
34. L. Lu, L. Zhang, H. Zeng, B. Xu, L.M. Wang, Y.M. Li, *J Alloy. Compd.*, 695 (2017) 1294.
35. Y. Li, J.P. Tu, X.H. Huang, H.M Wu, Y.F. Yuan, *Electrochim. Acta*, 52 (2006) 1383.